

5-10-91
E5983

NASA Technical Memorandum 103741

Mechanical Behavior and Failure Phenomenon of an In Situ- Toughened Silicon Nitride

Jonathan A. Salem, Sung R. Choi, Marc R. Freedman
Lewis Research Center
Cleveland, Ohio

and

Michael G. Jenkins
Oak Ridge National Laboratory
Oak Ridge, Tennessee

Prepared for the
43rd Annual Pacific Coast Meeting
sponsored by the American Ceramic Society
Seattle, Washington, October 25-27, 1990

NASA

MECHANICAL BEHAVIOR AND FAILURE PHENOMENON
OF AN IN SITU-TOUGHENED SILICON NITRIDE

Jonathan A. Salem, Sung R. Choi, Marc R. Freedman
NASA Lewis Research Center
Cleveland, Ohio

and

Michael G. Jenkins
Oak Ridge National Laboratory
Oak Ridge, Tennessee

ABSTRACT

The Weibull modulus, fracture toughness and crack growth resistance of an in situ-toughened, silicon nitride material used to manufacture a turbine combustor were determined from room temperature to 1371 °C. The material exhibited an elongated grain structure that resulted in improved fracture toughness, nonlinear crack growth resistance, and good elevated temperature strength. However, low temperature strength was limited by grains of excessive length (30 to 100 μm). These excessively long grains were surrounded by regions rich in sintering additives.

I. INTRODUCTION

The need for more fuel efficient transportation and lower engine emissions has made ceramics increasingly important materials for structural components of engines. Although the high temperature strength of ceramics has been advantageous, the low fracture toughness and poor reliability has been an impediment. Many methods of toughening ceramics have been attempted, however, the simplest method has been microstructural texturing or in situ toughening.

The mechanical properties of components made from in situ-toughened ceramics are controlled by the processing methods used in production. Thus, reliability analysis and life prediction of such ceramic structural components requires design data determined directly from components or access to relatively large experimental data

bases. Presently, data bases for such materials are limited. The objective of this work was to determine the mechanical properties and failure behavior of an in situ-toughened, silicon nitride material* processed in the form of a turbine combustor. The mechanical properties were subsequently used for reliability analysis (Refs. 1 and 2).

II. EXPERIMENTAL PROCEDURES

Material

A mixture of silicon nitride powder (Si_3N_4), sintering aids and a polymeric binder were milled in 50-l polyethylene jar with Si_3N_4 media for 3 days. The resulting slurry was separated from the media, dried and granulated. The granulated powder was cold isostatically pressed at 100 MPa to form a cylindrical combustor. The combustor was green machined to near final shape, dewaxed and then sintered in a nitrogen atmosphere. Final machining produced the combustor shown in Fig. 1. Typical microstructure is exhibited in Fig. 2. The grain structure was delineated with a modified plasma etching procedure (Ref. 3). No anisotropy was observed in metallographic sections of transverse and longitudinal orientations.

Mechanical Testing

Young's modulus and Poisson's ratio between room temperature and 1400 °C were determined by sonic resonance in accordance with ASTM method C848-76 (Ref. 4). Young's modulus was also determined at room temperature by strain gaging a four-point bend specimen.

Test specimens for strength and fracture toughness measurements were machined from the combustor and heat treated in air at 1150 °C for 1.5 hr to relieve residual stress and heal machining damage. Four-point bend strength was determined at temperatures of 25, 1000, and 1371 °C at a displacement rate of 0.5 mm/min. The

*Kyocera SN251 silicon nitride, Kyocera Corp., Kyoto, Japan.

strength specimens measured 3 x 4 mm in height and width, and the inner and outer spans of the flexure fixture were 10 and 30 mm, respectively.

Fracture toughness was determined with the single-edged precracked-beam (SEPB) (Ref. 5), single-edged notched-beam (SENB) and chevron-notch (Ref. 6) methods in three-point bending. Specimens measured 3 x 4 x 30 mm in width, height and span, and the notch width of the SENB specimen was 0.050 mm. The Chevron-notch parameters α_0 and α_1 were 0.625 and 1.0, respectively. The stress intensity factor coefficient was determined with a slice model (Ref. 6) and an interlaminar shear factor of 0.1453. The SEPB specimens were tested at a displacement rate of 0.5 mm/min, and chevron-notch specimens were tested at 0.005 mm/min. The low displacement rate used for chevron-notch testing was required to insure stable crack extension. Such slow rates were successful in the testing of SiC/TiB₂ composites (Ref. 7).

Room temperature R-curve behavior was estimated using the indentation strength technique proposed by Krause (Ref. 8). The test specimens were 3 x 5.6 x 25 mm MOR bars. The center of the tensile surface was polished and indented with a Vickers microhardness indenter at loads ranging from 49 to 196 N. The subsequent strength tests of the indented samples were conducted using a four-point bend fixture with 9.5 and 20 mm spans and a displacement rate of 0.2 mm/min in room temperature air. Three specimens were tested at each indentation load.

III. RESULTS AND DISCUSSION

Young's Modulus and Poisson's Ratio

Young's modulus exhibited a continuous drop from 309 GPa at 25 °C to 281 GPa at 1371 °C, indicating a slight sensitivity to temperature. The Young's modulus determined from strain gage readings at 25 °C was 299 MPa, about 3 percent lower than the sonically determined value. Poisson's ratio varied about an average of 0.27 ± 0.04 between room temperature and 1400 °C.

Strength

Weibull parameters can be determined by the uncensored or the censored data technique (Refs. 9 and 10). For uncensored data the parameters are determined from

$$\ln \ln \left(\frac{1}{1 - F} \right) = m_r \ln \left(\frac{\sigma_f}{\sigma_r} \right) \quad (1)$$

where σ_f is the fracture strength, σ_r is the characteristic strength, m_r is the Weibull modulus and F is the cumulative failure probability based on

$$F = \frac{j - 0.3}{J + 0.4} \quad (2)$$

where J is the total number of specimens, and j is the specimen rank as assigned by ordering specimens from weakest to strongest. It should be noted that the characteristic strength is dependent on specimen volume and should not be confused with the scale parameter which is independent of volume.

For censored data, the specimens are also ordered from weakest to strongest, however, the parameters are determined by adding an extra increment of rank to account for the presence of two flaw populations. The extra increment of rank is given by

$$\Delta = \frac{(J + 1) - j_i}{1 + J_o} \quad (3)$$

where j_i is the previous ranking and J_o is the number of samples beyond the present censored set. The adjusted ranking is determined by adding the increment determined from Eq. (3) to the previous ranking. The associated failure probability and censored Weibull parameters are determined from Eqs. (1) and (2) and the adjusted rank.

Failures were censored by location of the origin (surface connected flaws versus volume flaws), regardless of their processing source or nature (e.g., grain, pore, or

surface damage). Flaw location as well as its nature were determined with optical microscopy or scanning electron microscopy (SEM) as necessary.

Summaries of bend strength test results for both uncensored and censored data are given in Tables I and II, respectively. Strength decreased from an average ($\bar{\sigma}_f$) of 671 ± 41 MPa at room temperature to 520 ± 54 MPa at 1371°C , with a corresponding decrease of Weibull modulus from 18.90 to 11.25 (Table I). All observed failure origins were either large, 30 to $100\ \mu\text{m}$ grains with hexagonal cross-sections, or 15 to $70\ \mu\text{m}$ diameter pores. The coarse grains were frequently connected to glassy regions. These regions were analyzed with energy dispersive analysis and determined to be rich in sintering additives. Failure origins of different natures and locations are shown in Fig. 3, and a glassy region attached to a coarse grain is shown in Fig. 4.

The population of volume type failures observed at 25 and 1000°C was insufficient for accurate statistical characterization, however, at 1371°C nearly 50 percent of the specimens failed from volume flaws. This increase in incidence of volume failures with increasing test temperature may indicate a further healing of surface connected flaws during heating of the specimens to test temperature, and possibly a softening of the glassy phases surrounding grains of excessive length.

Weibull distributions (least squares) of bend strength for surface and volume flaws, determined using Eq. (3), are illustrated in Figs. 5(a) and (b), respectively. Both the maximum likelihood and least squares (LS) methods produced similar statistical parameters for censored data. Analysis of uncensored and censored data by the least squares method resulted in similar Weibull parameters, as shown in Table II for measurements at 1371°C . As noted above, testing at 25 and 1000°C resulted in too few volume failures for accurate comparison. Determination of the Weibull parameters for volume failure at low temperature may require either tensile testing or a large number of bend tests per condition.

Fracture Toughness

Fracture toughness results are summarized in Table III. Room temperature fracture toughness measured with the chevron-notch and the SEPB methods were comparable.

Fracture toughness, measured with the chevron-notch, decreased with temperature to 1200 °C. However, at 1371 °C the fracture toughness appeared to increase substantially. The corresponding load-displacement behavior became severely nonlinear with a much higher maximum load than exhibited by lower temperature tests. This maximum was followed by a large, residual load bearing ability and incomplete failure of the specimen. Measurements with the SENB at 1371 °C were much lower and comparable to values measured with the chevron-notch at 1200 °C. The SEPB specimen could not be used at elevated temperature because of precrack healing.

Typical room temperature fracture topography of chevron-notch and SEPB specimens is illustrated in Fig. 6. Although some of the very large, elongated grains oriented normal to the crack plane were pulled out, a more typical occurrence was cleavage without deflection of the crack path. Grains oriented at low angles were partially separated from the matrix prior to cleavage. Small, well bonded grains (<10 μm) failed in groups with grains extending out of the fracture surfaces.

Fracture surfaces of chevron-notch specimens tested at 1371 °C are shown in Figs. 7(a) and (b). The cracked region, shown in Fig. 7(a) was heavily oxidized with some grains protruding out of the oxide layer. The crack tip region where the crack stalled, shown in Fig. 7(b), exhibited a relatively large concentration of exposed grains. Evidently, the crack stalled due to deformation and hinging of the ligament. The stalled crack was oxidized and the long, favorably oriented grains near the crack tip were pulled apart by viscous deformation of the grain boundaries. The deformation hinging thus resulted in the high maximum and residual loads displayed, and the high, apparent fracture toughness. The grain pullout was indicative of

deformation instead of bridging, as high apparent toughness was also observed for fine grained silicon nitrides (Ref. 11).

R-Curve Behavior and Its Relation to Weibull Modulus

Damage or flaw tolerance that results from an increasing resistance to stable crack propagation is a desirable property for structural ceramics. Krause (Ref. 8) has shown that R-curve behavior can be evaluated from indentation strength data, assuming that the fracture resistance (K_r) is related to the crack length (c) by a power-law relationship. The fracture resistance and the indentation strength (σ_f) relations are expressed by

$$K_r = kc^\tau \quad (4)$$

$$\sigma_f = \frac{k(3 + 2\tau)}{4\beta} \left[\frac{4P\Gamma}{k(1 - 2\tau)} \right]^{(2\tau-1/2\tau+3)} \quad (5)$$

where k and τ are constants, Γ and β are the dimensionless quantities associated with the residual contact stress intensity and the crack geometry (defined in $K_I = \beta\sigma\sqrt{c}$, where K_I is the mode I stress intensity factor and σ is the applied stress) respectively, and P is the indentation load. When $\tau = 0$, Eq. (5) reduces to the case of no crack resistance toughening. Also, $K_r = K_{IC}$ for $\tau = 0$. The parameter τ was evaluated from the best-fit slope of the $\text{Log } \sigma_f$ - $\text{Log } P$ data shown in Fig. 8. The constant k was evaluated from Eq. (4) with the estimated τ and the toughness value obtained with the indentation strength method (Ref. 12) for a crack size of $c = 102 \mu\text{m}$.

The R-curve estimation is presented in Fig. 9, where the fracture resistance curve is plotted as a function of the crack size based on Eq. (4). For illustrative purposes, the fracture resistance curve for a silicon nitride** with an equiaxed microstructure (Fig. 10) is included (Ref. 13). It can be seen from Fig. 9 that the

**Norton 6 percent yttrium Si_3N_4 , Ref. 11.

in situ-toughened material exhibits strong R-curve behavior with a toughening exponent of $\tau = 0.126$; whereas the material with an equiaxed microstructure exhibits a flat R-curve with a negligibly small exponent of $\tau = 0.027$, and a lower level of K_{Ic} . The elongated grain morphology not only increased the fracture toughness, but imparted crack growth resistance to silicon nitride. Similar observations of rising R-curve behavior ($\tau = 0.1$ to 0.22) and improved fracture toughness were found in other in situ-toughened silicon nitrides (Refs. 14 and 15).

Ceramics with a rising R-curve have been experimentally shown to exhibit a higher Weibull modulus as compared to ceramics with a flat R-curve. Kendall et al. (Ref. 16), Cook and Clarke (Ref. 17), and Shetty and Wang (Ref. 18) made attempts to develop closed form solutions for the modified Weibull parameters based on fracture mechanics principles and two-parameter Weibull statistics. A similar derivation of the modified Weibull parameters for the R-curve enhanced material, based on the procedure used by Shetty and Wang (Ref. 18), was made in this study and found to yield

$$m_r = \frac{m_o}{1 - 2\tau} \quad (6)$$

and

$$\sigma_r = \frac{kK_{Ic}^{2\tau-1}}{\sigma_o^{2\tau-1} \beta^{2\tau}} \quad (7)$$

where m_r and σ_r are the Weibull modulus and characteristic strength of the material with R-curve behavior (i.e., those measured in this study), respectively, and m_o and σ_o are the Weibull modulus and characteristic strength for a flat R-curve material with the same flaw distribution. The Weibull modulus m_r is the same as that derived by Kendall et al. (Ref. 16) or Shetty and Wang (Ref. 18). However, the characteristic strength, σ_r is different from the one derived by Shetty

and Wang (Ref. 18) by a factor of $(\pi\beta^2/4)^{-\tau}$. Note that when $\tau = 0$ the parameters reduce to the m_0 and σ_0 for the flat R-curve material. It also should be noted that the characteristic strength σ_r in Eq. (7) is not an explicit function of the given material, but rather depends on the functional form that is chosen to represent K_{IC} .

Equation (6) shows that the Weibull modulus increases with increasing toughening exponent. For the previously evaluated exponent $\tau = 0.126$ and surface Weibull modulus of $m_r = 18.36$, the Weibull modulus of a flat R-curve material with the same surface flaw distribution is back-calculated as $m_0 = 14$, a value typical of the upper range for monolithic silicon nitrides. This indicates that R-curve behavior increased the Weibull modulus by 34 percent as compared to a material with the same flaw distribution and a flat R-curve. The Weibull modulus for surface flaws, $m_r = 18.36$, was used in the above calculation because the value of τ was derived from surface indentations cracks, and the R-curve is not considered unique for crack extension from different flaws. However, if the value of τ associated with stable crack extension from volume flaws is known (the same growth pattern), then the analysis should be applicable to volume flaws as well as surface flaws.

Although several simplifying assumptions were made in the above analysis, this approach gives a quantitative insight to the increased Weibull modulus observed for materials with rising R-curves.

Crack Trajectory

In an attempt to explain the greater room temperature fracture toughness and crack growth resistance of the in situ-toughened material relative to the silicon nitride with an equiaxed microstructure, indentation cracks (Vickers indentation load = 98 N) were placed in polished sections of both materials. The crack trajectories, as observed by SEM, are shown in Fig. 11. The cracks traversed through the equiaxed microstructure with little deflection, but occasional bridging was

apparent. In the in situ-toughened material, however, the cracks followed a very tortuous path through the microstructure.

The crack path relative to the grain boundaries of the in situ-toughened material is illustrated in Fig. 12. The crack passed through the boundaries of small grains as well as large grains oriented at low angles, resulting in crack deflection, interlocking, and bridging behavior analogous with whisker pullout. Note the wedging of the elongated grain relative to surrounding material (arrow A), and the resultant, secondary cracking (arrow B). Long grains oriented at large angles to the crack path were cleaved (arrow C). This crack interaction with the elongated grain structure may account for the improved fracture toughness and rising crack growth resistance of the in situ-toughened material relative to the material with an equiaxed microstructure.

CONCLUSIONS

Silicon nitride with an elongated microstructure exhibited good elevated temperature strength and a high Weibull modulus. Ultimate strength of the material was limited by excessively large, 30 to 100 μm grains, or 15 to 70 μm diameter pores. The excessively long grains were developed by a nonuniform distribution of sintering additives. The room temperature failure origins were predominately surface connected flaws. At 1371 °C the failure origins were frequently within the volume and the Weibull modulus decreased to approximately 11 from a room temperature value of 19. The increased incidence of volume failure and lower Weibull modulus were probably due to softening of the glassy secondary phases surrounding large grains, healing of surface flaws, and a possible loss of crack growth resistance.

The SEPB and chevron-notch fracture toughness test methods resulted in similar measured values at room temperature. At 1371 °C, load rate and deformation effects unfavorably influenced fracture toughness measurements made with the chevron-notch flexure bar. Crack growth resistance at room temperature ranged from 6.5 to 9 MPa

within a 300 μm crack extension, resulting in a 34 percent, estimated enhancement of the Weibull modulus.

The improved fracture toughness, crack growth resistance and Weibull modulus were attributed to the elongated grain structure, which resulted in significant crack deflection and bridging, as compared to that of a material with an equiaxed microstructure.

ACKNOWLEDGMENT

The authors would like to thank Oak Ridge National Laboratory for funding under contract DE-AI05-87OR21749.

REFERENCES

1. J.A. Salem, J. Manderscheid, M. Freedman, and J. Gyekenyesi, "Reliability Analysis of a Ceramic Turbine Combustor," Submitted to J. Gas Turbines Eng. (1990).
2. J.P. Gyekenyesi, J. Eng. Gas Turbine Power **108**, (1986) 540.
3. K.N. Siebein and W.M. Lovington, in "Microstructural Science," Vol. 16: "Metallography of Advance Materials," edited by H.J. Cialone (International Metallographic Society, Columbus, OH, 1988) p. 319.
4. "Young's Modulus, Shear Modulus, and Poisson's Ratio for Ceramic Whitewares by Resonance," ASTM Standard Test Method C848-88. American Society for Testing and Materials, Philadelphia, PA.
5. T. Nose and T. Fujii, J. Am. Ceram. Soc. **71** (1988) 328.
6. D. Munz, R.T. Bubsey, and J.L. Shannon, Jr., J. Am. Ceram. Soc. **63** (1980) 300.
7. M.J. Jenkins, J.A. Salem, and S.G. Seshardri, J. Comp. Mater. **23**, (1989) 77.
8. K.F. Krause, J. Am. Ceram. Soc. **71** (1988) 338.
9. K. Jakus, J.E. Ritter, Jr., T. Service, and D. Sonderman, J. Am. Ceram. Soc., (1981) C-174.
10. S.A. Szatmary, J.P. Gyekenyesi, and N.N. Nemeth, NASA Technical Memorandum 103247 (1990).

11. J.A. Salem, NASA Technical Memorandum 102423, 1990.
12. P. Chantikul, G.R. Anstis, B.R. Lawn, and D.B. Marshall, J. Am. Ceram. Soc. **64** (1981) 539.
13. S.R. Choi and J. Salem, "Strength and Fracture Toughness Properties of Whisker Reinforced Silicon Nitride Matrix Composite and Monolithic Silicon Nitride," Presented at the Symposium on Composites sponsored by American Ceramics Society, Orlando, Fla., Nov. 12-15, 1990.
14. J.E. Ritter, S.R. Choi, K. Jakus, P.J. Whalen, and R.G. Rateick, "Effect of Microstructure on the Erosion and Impact Damage of Sintered Silicon Nitride," To be published in J. Mater. Sci. (1991).
- 15 C.W. Li and Y. Yamanis, Ceram. Eng. Sci. Proc. **10** (1989) 632.
16. K. Kendall and N.M. Ashford, S.R. Tan, and J.D. Birchall, J. Mater. Res. **1** (1986) 120.
17. R.F. Cook and D.R. Clarke, Acta Metall. **36** (1988) 555.
18. D.K. Shetty and J.S. Wang, J. Am. Ceram. Soc. **72** (1988) 1158.

TABLE I. - AVERAGE STRENGTH, UNCENSORED WEIBULL PARAMETERS (LS),
AND NATURE OF FAILURE ORIGINS

Temperature °C	$\bar{\sigma}_f^a$, MPa	σ_r , MPa	Weibull modulus	Flaw location	Flaw type	Number of occurrences
25	671 (41)	690	18.90	Surface	Grain	14
				Surface	Pore	6
				Surface	ND ^b	6
				Volume	Grain	2
				Volume	Pore	0
				Volume	ND ^b	1
				Undetermined		2
1000	469 (47)	590	14.05	Surface	Grain	15
				Surface	Pore	2
				Surface	ND ^b	0
				Volume	Grain	0
				Volume	Pore ^b	0
				Volume	ND ^b	10
1371	520 (54)	544	11.25	Surface	Grain	24
				Surface	Pore	5
				Volume	Grain	17
				Volume	Pore	4

^aTotal specimen population, the numbers in parenthesis indicate 1.0 standard deviation.

^bFlaw nature was not determined (ND) for expediency.

TABLE II. - CENSORED WEIBULL PARAMETERS

Temperature, °C	Flaw ^a location	Number of specimens	Least squares fit		Maximum likelihood	
			σ_r , MPa	m_r	σ_r , MPa	Weibull modulus m_r
25	S	26	694	18.36	694	18.65
	V	3	^b 752	21.44	749	32.44
	U	2	---	-----	---	-----
1000	S	26	591	13.78	592	13.33
	V	1	---	-----	---	-----
	U	0	---	-----	---	-----
1371	S	29	565	10.12	574	8.86
	V	21	585	13.95	585	15.31
	U	0	---	-----	---	-----

^aS = surface flaw; V = volume flaw; U = unknown origin.

^bEstimated for three data points.

TABLE III. - FRACTURE TOUGHNESS

Test method	Temperature, °C	Number of tests	K_{IC} , MPa \sqrt{m}
Chevron notch	25	5	7.9±0.4
	800	5	7.1±0.7
	1000	3	6.9±0.3
	1200	4	6.0±0.3
	1371	2	10.4±0.5
SEPB	25	7	7.4±0.5
SENB	1371	4	6.1±0.4



Figure 1.—View of the silicon nitride combustor.

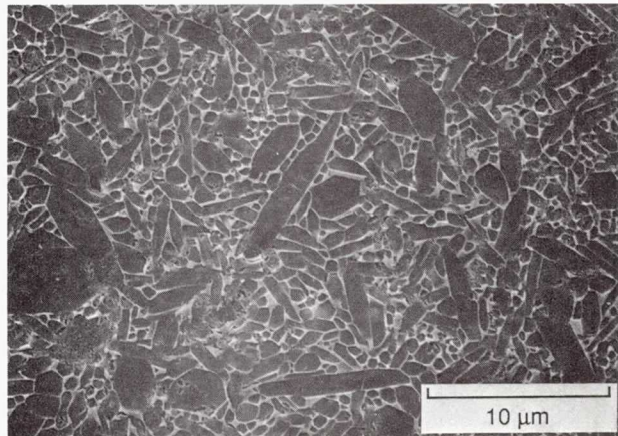


Figure 2.—Plasma etched microstructure of in situ-toughened silicon nitride.

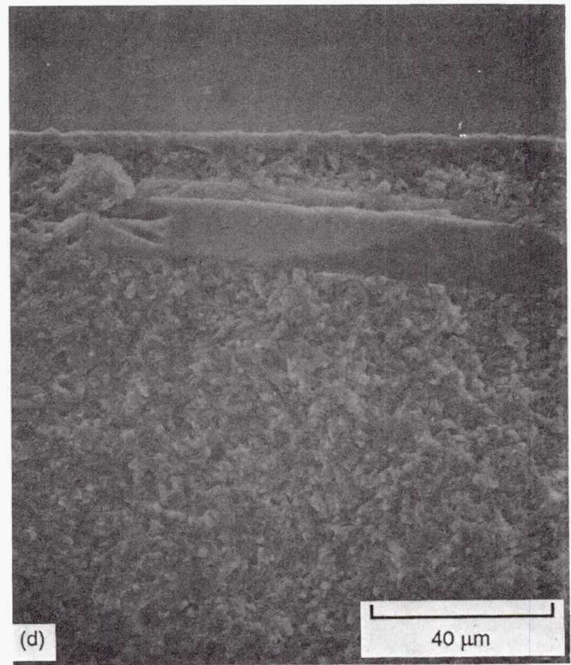
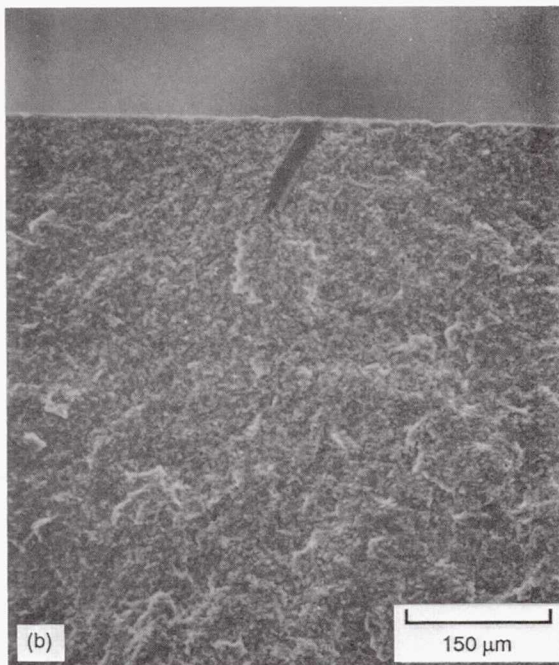
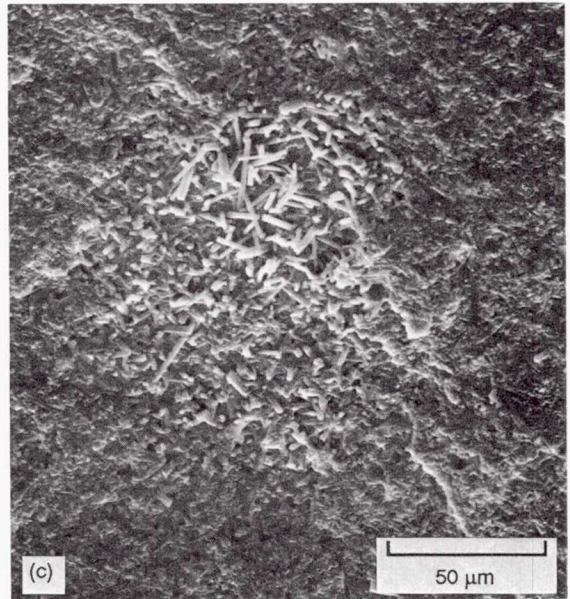
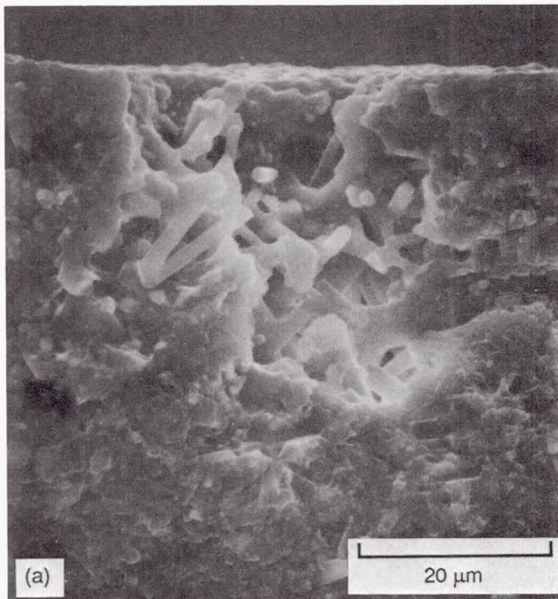


Figure 3.—Typical failure origins: (a) surface connected pore, (b) large, surface connected grain, (c) volume pore, and (d) large volume grain.



Figure 4.—Glassy region connected to a large grain that induced strength failure.

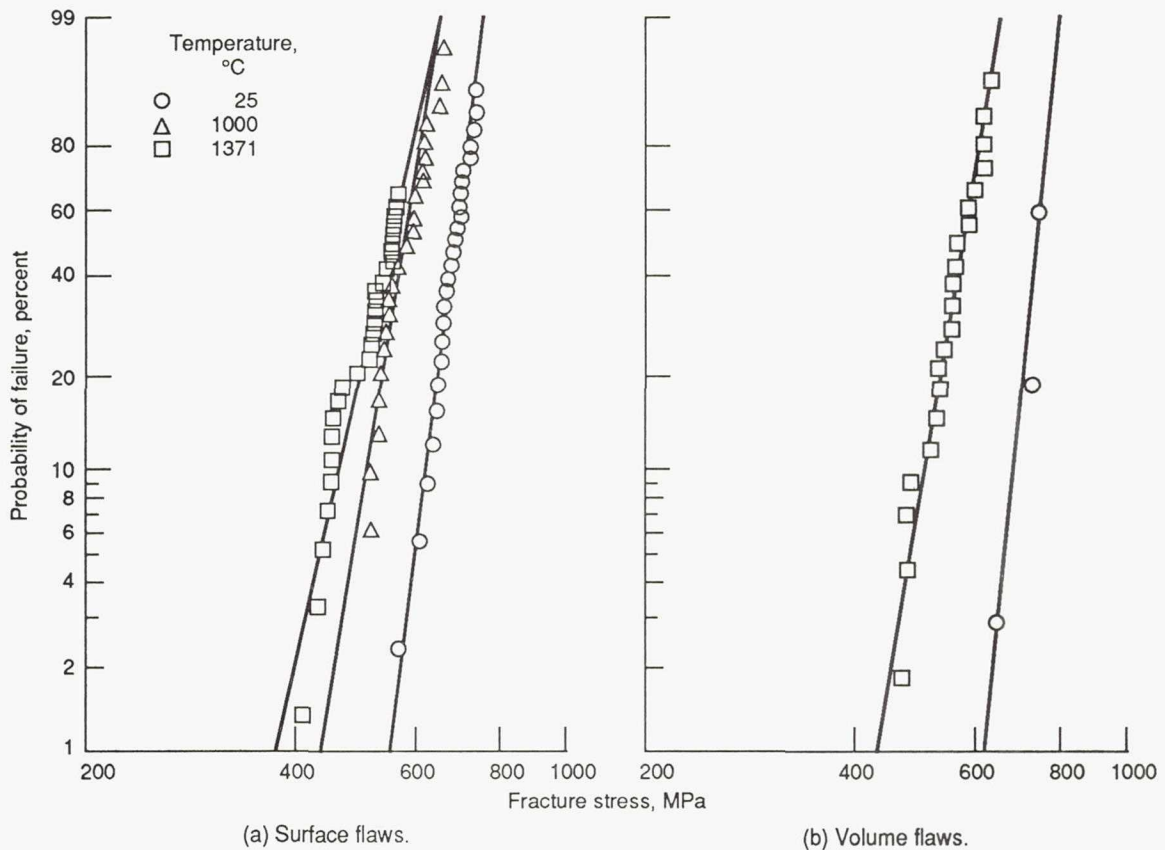


Figure 5.—Weibull distributions (least squares).

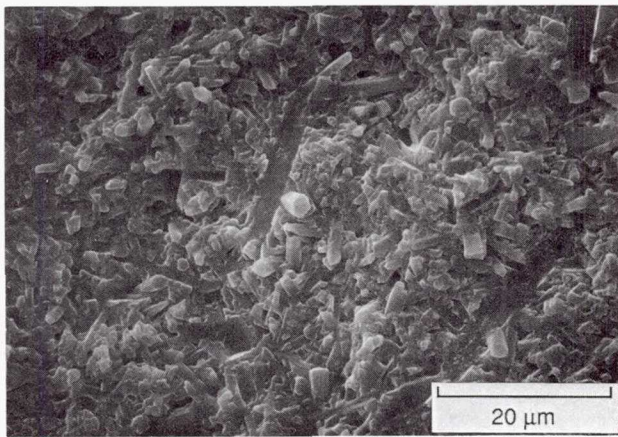


Figure 6.—Room temperature fracture toughness topography.

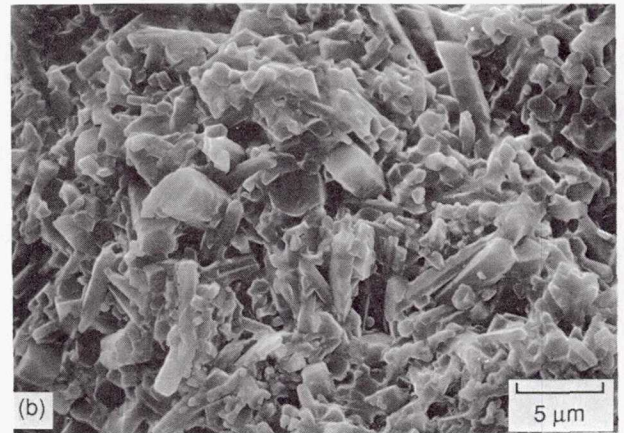
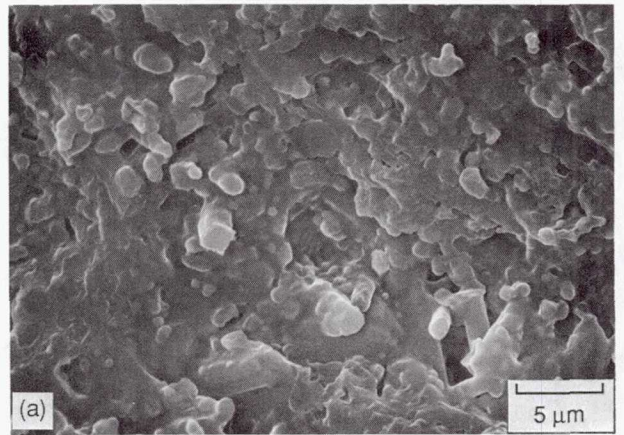


Figure 7.—Chevron-notch fracture topography for 1371 °C. (a) Oxidized wake region (b) crack tip.

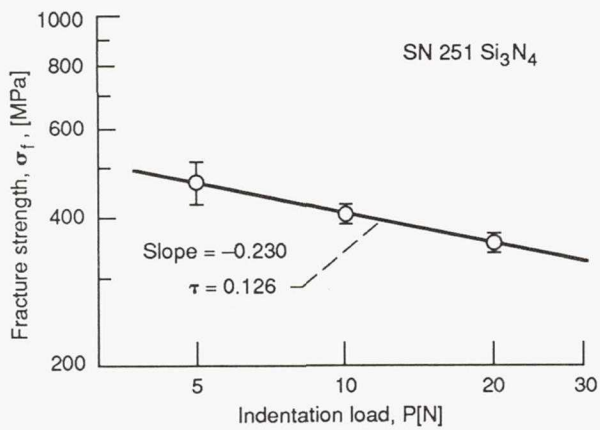


Figure 8.—Fracture strength as a function of indentation load. Error bar indicates ± 1.0 standard deviation.

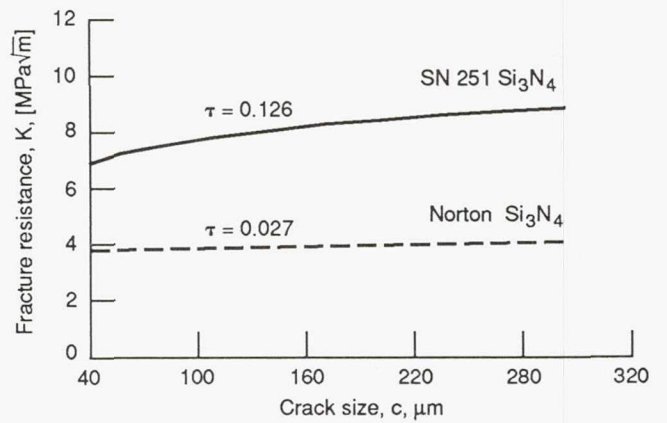


Figure 9.—Predicted fracture resistance curves for in situ-toughened material and material with an equiaxed grain structure.

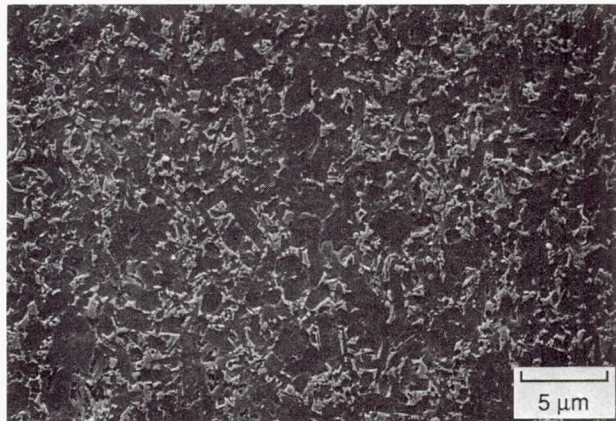


Figure 10.—Plasma etched microstructure of a 6 percent yttrium silicon nitride with an equiaxed grain structure.

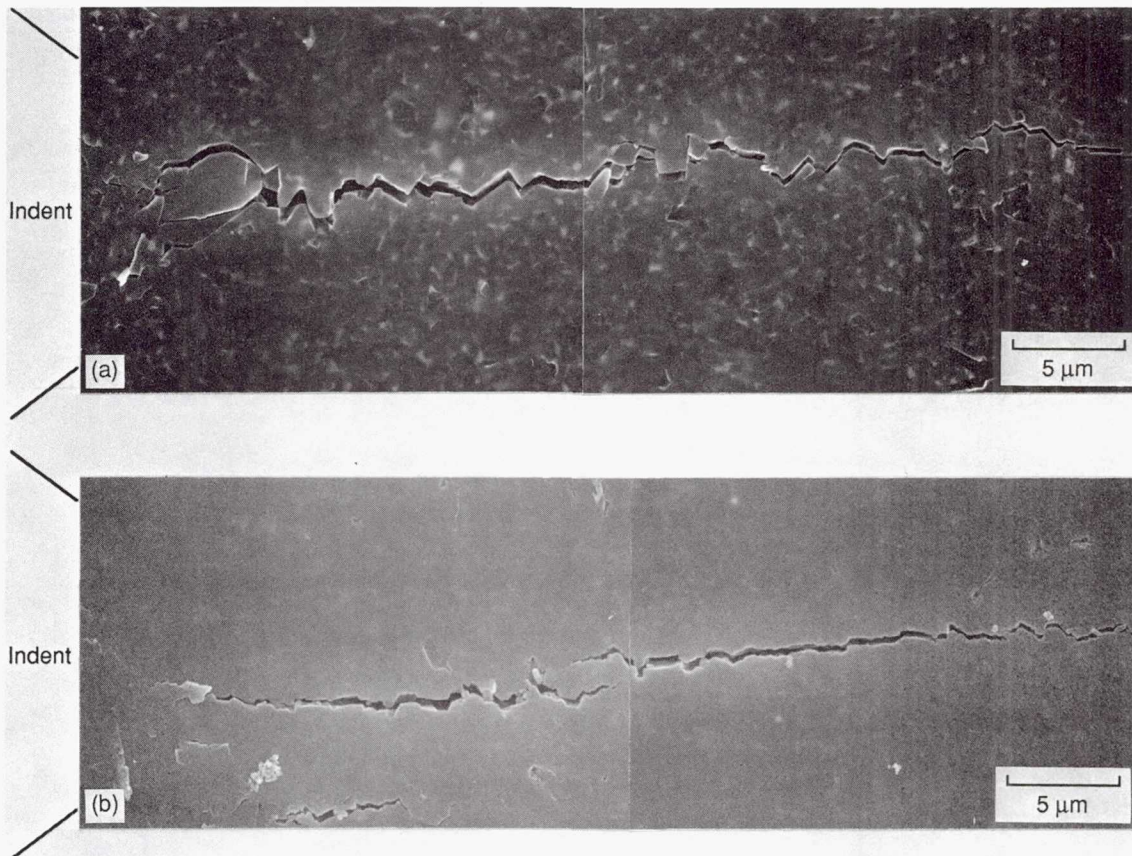


Figure 11.—Indentation crack trajectory for (a) in situ-toughened silicon nitride and in (b) silicon nitride with an equiaxed microstructure.

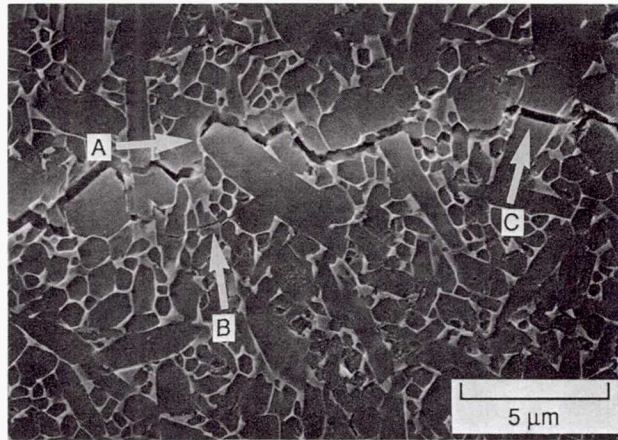


Figure 12.—Indentation crack trajectory for etched, in situ-toughened silicon nitride.

1. Report No. NASA TM-103741		2. Government Accession No.		3. Recipient's Catalog No.	
4. Title and Subtitle Mechanical Behavior and Failure Phenomenon of an In Situ-Toughened Silicon Nitride				5. Report Date	
				6. Performing Organization Code	
7. Author(s) Jonathan A. Salem, Sung R. Choi, Marc R. Freedman, and Michael G. Jenkins				8. Performing Organization Report No. E-5983	
				10. Work Unit No. 505-63-1M	
9. Performing Organization Name and Address National Aeronautics and Space Administration Lewis Research Center Cleveland, Ohio 44135-3191				11. Contract or Grant No.	
				13. Type of Report and Period Covered Technical Memorandum	
12. Sponsoring Agency Name and Address National Aeronautics and Space Administration Washington, D.C. 20546-0001				14. Sponsoring Agency Code	
15. Supplementary Notes Prepared for the 43rd Annual Pacific Coast Meeting sponsored by the American Ceramic Society, Seattle, Washington, October 25-27, 1990. Jonathan A. Salem, Sung R. Choi, and Mark R. Freedman, NASA Lewis Research Center; Michael G. Jenkins, Oak Ridge National Laboratory, Oak Ridge, Tennessee. Responsible person, Jonathan A. Salem, (216) 433-3313.					
16. Abstract The Weibull modulus, fracture toughness and crack growth resistance of an in situ-toughened, silicon nitride material used to manufacture a turbine combustor were determined from room temperature to 1371 °C. The material exhibited an elongated grain structure that resulted in improved fracture toughness, nonlinear crack growth resistance, and good elevated temperature strength. However, low temperature strength was limited by grains of excessive length (30 to 100 μm). These excessively long grains were surrounded by regions rich in sintering additives.					
17. Key Words (Suggested by Author(s)) Weibull modulus; Fracture toughness; In situ-toughened; Crack growth resistance; Strength; Silicon nitride			18. Distribution Statement Unclassified - Unlimited Subject Category 27		
19. Security Classif. (of this report) Unclassified		20. Security Classif. (of this page) Unclassified		21. No. of pages 20	22. Price* A03